



Deposited via The University of Leeds.

White Rose Research Online URL for this paper:

<https://eprints.whiterose.ac.uk/id/eprint/164878/>

Version: Accepted Version

---

**Article:**

Xing, C, Li, K, Zhang, L et al. (2020) Optimal Compensation Control of Railway Co-phase Traction Power Supply Integrated with Renewable Energy Based on NSGA-II. IET Renewable Power Generation, 14 (18). pp. 3668-3678. ISSN: 1752-1416

<https://doi.org/10.1049/iet-rpg.2020.0130>

---

© The Institution of Engineering and Technology 2020. All rights reserved. This paper is a postprint of a paper submitted to and accepted for publication in IET Renewable Power Generation and is subject to Institution of Engineering and Technology Copyright. The copy of record is available at the IET Digital Library.

**Reuse**

Items deposited in White Rose Research Online are protected by copyright, with all rights reserved unless indicated otherwise. They may be downloaded and/or printed for private study, or other acts as permitted by national copyright laws. The publisher or other rights holders may allow further reproduction and re-use of the full text version. This is indicated by the licence information on the White Rose Research Online record for the item.

**Takedown**

If you consider content in White Rose Research Online to be in breach of UK law, please notify us by emailing [eprints@whiterose.ac.uk](mailto:eprints@whiterose.ac.uk) including the URL of the record and the reason for the withdrawal request.

---

# Optimal Compensation Control of Railway Co-phase Traction Power Supply Integrated with Renewable Energy Based on NSGA-II

Chen Xing<sup>1</sup>, Kang Li<sup>1\*</sup>, Li Zhang<sup>1</sup>, Wei Li<sup>2</sup>

<sup>1</sup> School of Electronic and Electrical Engineering, University of Leeds, Leeds, UK

<sup>2</sup> School of Traffic and Transportation Engineering, Central South University, Changsha, China

\* E-mail: K.Li1@leeds.ac.uk

**Abstract:** In railway traction power supply, the co-phase system with hybrid power quality conditioner (HPQC) is capable of tackling power quality issues caused by single-phase traction loads. To reduce the carbon emission, it is proposed to integrate renewable energy with the railway power supply, leading to a more complex system to model, design and control. This paper first investigates the modelling aspect of this new system. To reduce the operating capacity of HPQC while addressing the power unbalance, optimal design of the compensation scheme for co-phase system is formulated as a multi-objective optimization problem which is solved by the nondominated sorting genetic algorithm-II (NSGA-II). Furthermore, to eliminate the effect of errors arising from imperfect predictions of the loads and renewable power, a hybrid optimal compensation control is proposed, yielding full and optimal compensations. Comprehensive simulation studies, considering three operation modes that cover variable traction loads, renewable power, as well as regenerative braking power, are conducted. The simulation results confirm the validity of the proposed optimal compensation scheme, achieving an average of more than 20% reduction of the HPQC capacity compared to the full compensation scheme. Meanwhile, the power quality requirement is always satisfied, even in the presence of real-time prediction errors.

---

## 1 Introduction

The rapid development of high-speed rail is significantly increasing the capacity of rail transport worldwide, further facilitating the shift towards electrification and reduction of carbon emissions. The single-phase 50Hz/25kV AC power system has been widely applied in electrified traction systems [1]. Generally, in the feeder stations, a step-down transformer is connected between the three-phase power grid and two single-phase catenary overhead lines. Each single-phase provides power for one traction power supply arm, and an insulator is needed between adjacent power supply arms to prevent phase mixture. However, as the traction loads are dynamic, time-varying and distributed in different power supply arms, power unbalance caused by the negative sequence and harmonics in the line current and voltage usually exists [2–4]. Furthermore, there is a limit for the reactive power injected from the traction loads into the power grid due to the power factor limit imposed by the grid code.

To solve the power quality issues, various compensation schemes have been proposed, though only a few have been adopted in practice due to the high cost and complexity. The static synchronous compensator (STATCOM) is among the few compensation schemes that have been widely deployed at the three-phase side of the feeder stations [5]. However the reactive power and negative sequence current can still pass through the traction transformer, increasing the risks to the transformers. In [6], a novel co-phase traction power supply system was proposed, where the transformer configuration is still preserved but the insulator is removed. An active power compensator (APC) based on the back-to-back converter is applied and the full compensation control method is demonstrated. The negative sequence current is cancelled and the reactive power is compensated, thus achieving the system balance and unity power factor in the grid side. In [7], a new topology for co-phase railway system was also proposed. A 10MVA-rated co-phase system has been operated in China and the compensation performance has been validated [8]. But under this full compensation scheme, the APC provides half of the active power and full reactive power of the traction loads, which leads to a high operating capacity requirement. The current conduction power efficiency of converters is about 98% [9–11], therefore

a large amount of power loss is incurred due to the high operating capacity. To reduce the capacity while simultaneously improving the power quality is an important research topic. In [12], a partial compensation scheme is presented and the hybrid power quality conditioner (HPQC) is adopted in the co-phase system. The design, parameter selection and control method are introduced in [13–16]. In partial compensation, the HPQC only compensates part of the negative sequence current and reactive power to reduce the operating capacity. However, the fixed partial compensation strategy is not suitable for all traction loads. A partial compensation scheme adopted for a lower traction load may be inadequate for a higher load case. Hence it is vital to design optimal compensation solutions under different traction load conditions. These raise the needs to achieve the maximum reduction in required capacity while meeting the requirements for system balance and reactive power.

While the railway electrification and high speed rail applications have had profound societal impacts, the energy landscape has also significantly shifted with the significant penetration of renewable generation [17–21]. The optimal operation of electric railways integrated with renewable energy is also discussed in [22], though such an integration inevitably increases the complexity of the system. This paper investigates the integration scheme as illustrated in Fig. 1, where the renewable generation provides active power via the DC-link of the back-to-back converter. The batteries can smooth the variations in the power flow. The renewable generators work together with the grid to provide the necessary traction power.

To reduce the operating capacity of the HPQC as well as the power system unbalance, this paper proposes to formulate the compensation design as a multi-objective optimization problem which is then solved by the NSGA-II. The NSGA-II is a powerful multi-objective optimization method that has been successfully applied to many engineering problems, such as design of five-phase induction machines [23], control of wind turbines [24], and reducing the fuel consumption and operating costs of hybrid vehicles [25].

The remainder of the paper is organized as follows. Section 2 discusses the modelling of the co-phase system with renewable energy integration. While Section 3 presents the principles of full compensation. To identify the optimal compensation schemes under varying traction loads and renewable generations, the NSGA-II is applied.

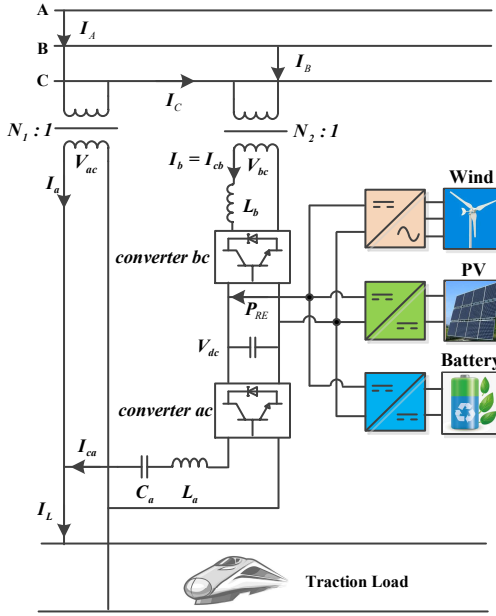


Fig. 1: Co-phase system with renewable energy integration

In Section 4, to achieve optimal compensation while mitigating the negative impacts of real-time prediction errors in the traction loads and the renewable power, a hybrid optimal compensation control is proposed. In section 5, the effectiveness of the NSGA-II optimization and the optimal control of the hybrid compensation are verified through numerical simulations. The results confirm that the optimal compensation can reduce the operating capacity of the HPQC as well as the power loss, while the power quality requirements are always met. Finally, section 6 concludes the paper.

## 2 Modelling of Co-phase System with Renewable Energy Integration

As illustrated in Fig. 1, the three-phase power supply from the grid is split into two single-phase channels by the V/V transformer, a most common transformer configuration. One single phase *ac* connects to the traction line directly to feed traction loads. The back-to-back HPQC is connected between phase *bc* and phase *ac*, which can achieve flexible power compensation and harmonic suppression. The HPQC is composed of two voltage converters and a capacitor to stabilize the DC voltage. In a renewable energy integrated co-phase system, renewable power is injected into the DC link through DC/DC or AC/DC converters. The detailed models and analysis are introduced below.

### 2.1 Conventional Co-phase System

For the conventional co-phase system without renewable energy, the phasor diagram is shown in Fig. 2(a). The analysis is under the fundamental frequency 50Hz. The three-phase voltages are denoted as  $\tilde{V}_A$ ,  $\tilde{V}_B$  and  $\tilde{V}_C$ . The secondary side voltages are  $\tilde{V}_{ac}$  and  $\tilde{V}_{bc}$  respectively. The voltage phasors are given in (1).

$$\begin{bmatrix} \tilde{V}_A \\ \tilde{V}_B \\ \tilde{V}_C \\ \tilde{V}_{ac} \\ \tilde{V}_{bc} \end{bmatrix} = \begin{bmatrix} V_A e^{j0} \\ V_B e^{-j\frac{2\pi}{3}} \\ V_C e^{j\frac{2\pi}{3}} \\ V_{ac} e^{-j\frac{\pi}{6}} \\ V_{bc} e^{-j\frac{\pi}{2}} \end{bmatrix} \quad (1)$$

$\tilde{I}_a$  and  $\tilde{I}_b$  are secondary side currents and define  $\tilde{I}_c = -\tilde{I}_a - \tilde{I}_b$ .  $\varphi_a$ ,  $\varphi_b$  and  $\varphi_c$  denote the phase angles at the grid side. The phase angle is positive if the phase voltage leads the current. The currents are given in (2).

$$\begin{bmatrix} \tilde{I}_a \\ \tilde{I}_b \\ \tilde{I}_c \end{bmatrix} = \begin{bmatrix} I_a e^{-j\varphi_a} \\ I_b e^{-j(\varphi_b + \frac{2\pi}{3})} \\ -\tilde{I}_a - \tilde{I}_b \end{bmatrix} \quad (2)$$

Since the traction loads are fed by phase *ac* and phase *bc* together, the traction power including active power  $P_L$  and reactive power  $Q_L$  can be expressed as (3).

$$\begin{aligned} \begin{bmatrix} P_L \\ Q_L \end{bmatrix} &= \begin{bmatrix} V_{ac} I_L \cos \varphi_L \\ V_{ac} I_L \sin \varphi_L \end{bmatrix} = \begin{bmatrix} V_{ac} (I_{ap} + I_{cap}) \\ V_{ac} (I_{aq} + I_{caq}) \end{bmatrix} \\ &= \begin{bmatrix} V_{ac} I_{ap} + V_{bc} I_{cbp} \\ V_{ac} I_{aq} + V_{ac} I_{caq} \end{bmatrix} = \begin{bmatrix} V_{ac} (I_{ap} + \frac{N_1}{N_2} I_{cbp}) \\ V_{ac} (I_{aq} + I_{caq}) \end{bmatrix} \end{aligned} \quad (3)$$

where  $\cos \varphi_L$  is the load power factor.  $I_L$  is the traction load current.  $N_1$  and  $N_1$  are the transformer ratios.  $I_{ap}$ ,  $I_{cap}$  and  $I_{cbp}$  are active currents.  $I_{aq}$ ,  $I_{caq}$  and  $I_{cbq}$  are reactive currents. According to (3), the following can be easily derived

$$\begin{cases} I_{ap} = I_L \cos \varphi_L - \frac{N_2}{N_1} I_{cbp} \\ I_{cap} = \frac{N_2}{N_1} I_{cbp} \end{cases} \quad (4)$$

Further, based on Fig. 2(a), the reactive currents are given as

$$\begin{cases} I_{aq} = \tan(\frac{\pi}{6} - \varphi_a) (I_L \cos \varphi_L - \frac{N_2}{N_1} I_{cbp}) \\ I_{caq} = I_L \sin \varphi_L + \tan(\frac{\pi}{6} - \varphi_a) (I_L \cos \varphi_L - \frac{N_2}{N_1} I_{cbp}) \\ I_{cbq} = \tan(\frac{\pi}{6} + \varphi_b) I_{cbp} \end{cases} \quad (5)$$

Combining (4) and (5) yields

$$\begin{bmatrix} I_{ap} \\ I_{aq} \\ I_{cap} \\ I_{caq} \\ I_{cbp} \\ I_{cbq} \end{bmatrix} = \begin{bmatrix} I_L \cos \varphi_L - \frac{N_2}{N_1} I_{cbp} \\ \tan(\frac{\pi}{6} - \varphi_a) (I_L \cos \varphi_L - \frac{N_2}{N_1} I_{cbp}) \\ \frac{N_2}{N_1} I_{cbp} \\ I_L \sin \varphi_L + \tan(\frac{\pi}{6} - \varphi_a) (I_L \cos \varphi_L - \frac{N_2}{N_1} I_{cbp}) \\ I_{cbp} \\ \tan(\frac{\pi}{6} + \varphi_b) I_{cbp} \end{bmatrix} \quad (6)$$

### 2.2 Co-phase System with Renewable Energy Integration

When the renewable energy is integrated into the co-phase system, three main operation modes are considered:

- Mode 1: When the traction load is positive and the traction power requirement  $S_L$  is greater than the renewable power  $P_{RE}$ , the traction power is supplied by both the grid and the renewable generation.
- Mode 2: When the traction load is positive and the traction power requirement  $S_L$  is less than renewable power  $P_{RE}$ , the traction power requirement is met by renewable energy. The excessive renewable power is fed into the power grid.
- Mode 3: When the traction power is negative, i.e. the train is operated in the regeneration mode. The regenerative power from trains and renewable power are all fed to the power grid.

The power flow of the three operation modes are shown in Fig. 3. Due to the renewable energy integration, the phasor diagram is revised accordingly as shown in Fig. 2(b). Fig. 2(b) is a generalized phasor diagram. Even though the magnitude and direction of the phasors are variable in this diagram, the phasor relations remain the same. Thus the analysis below is applicable to all the three operation modes. Take the power flow direction in Fig. 3(a) as the reference direction and based on the power balance principle, (7) can be obtained, where  $P_{RE}$  represents the renewable power.

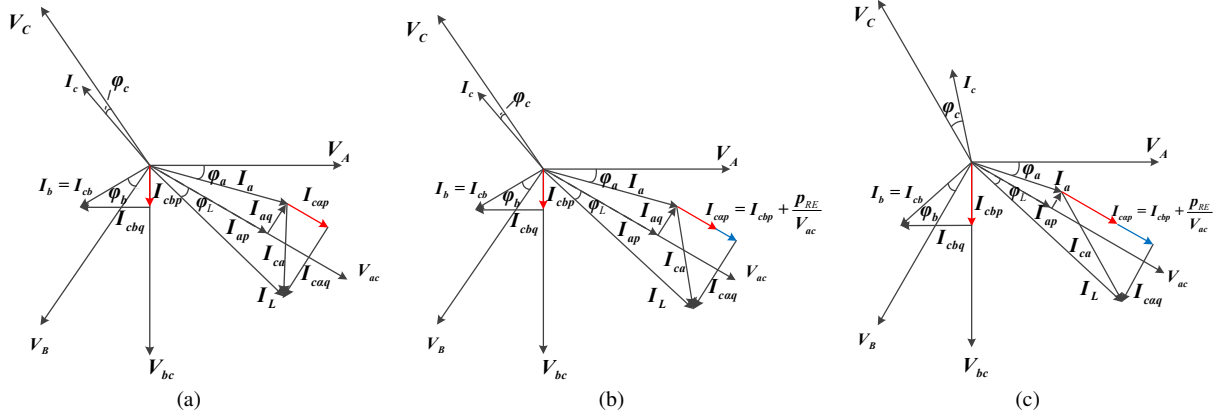


**Fig. 2:** Phasor diagrams of co-phase system. (a) Conventional co-phase system. (b) Co-phase system with renewable energy integration. (c) Co-phase system under full compensation.

$$\begin{aligned}
 P_L &= P_a + P_{ca} = P_a + P_{cb} + P_{RE} \\
 &= V_{ac}(I_{ap} + I_{cap}) = V_{ac}I_{ap} + V_{bc}I_{cbp} + P_{RE} \\
 &= V_{ac}(I_{ap} + \frac{N_2}{N_1}I_{cbp} + \frac{P_{RE}}{V_{ac}}) \\
 &= V_{ac}I_L \cos \varphi_L
 \end{aligned} \quad (7)$$

According to (7), (6) can be revised to (8). In order to simplify the analysis, it is assumed that the transformer ratio  $N_1 = N_2$ . In Fig. 2(b), the phase angle  $\varphi_c$  satisfies (9).

$$\begin{aligned}
 \tan \varphi_c &= \frac{\sin \varphi_c}{\cos \varphi_c} = \frac{I_{cq}}{I_{cp}} \\
 &= \frac{-I_a \sin(\frac{\pi}{3} - \varphi_a) + I_b \sin(\frac{\pi}{3} + \varphi_b)}{I_a \cos(\frac{\pi}{3} - \varphi_a) + I_b \cos(\frac{\pi}{3} + \varphi_b)} \\
 &= \frac{-\frac{I_{ap}}{\cos(\frac{\pi}{6} - \varphi_a)} \sin(\frac{\pi}{3} - \varphi_a) + \frac{I_{cbp}}{\cos(\frac{\pi}{6} + \varphi_b)} \sin(\frac{\pi}{3} + \varphi_b)}{\frac{I_{ap}}{\cos(\frac{\pi}{6} - \varphi_a)} \cos(\frac{\pi}{3} - \varphi_a) + \frac{I_{cbp}}{\cos(\frac{\pi}{6} + \varphi_b)} \cos(\frac{\pi}{3} + \varphi_b)}
 \end{aligned} \quad (9)$$

Substituting (8) into (9), the relationships between  $I_{cbp}$  and  $\varphi_a$ ,  $\varphi_b$  and  $\varphi_c$  can be derived as in (10), where  $K$  is the compensation factor determined by  $\varphi_a$ ,  $\varphi_b$  and  $\varphi_c$ . Based on (8) and (10), the converter compensation currents can be calculated as (11).

$$\begin{bmatrix} I_{cap} \\ I_{caq} \\ I_{cbp} \\ I_{cbq} \end{bmatrix} = \begin{bmatrix} K I_L \cos \varphi_L + (1 - K) \frac{P_{RE}}{V_{ac}} \\ K_a (I_L \cos \varphi_L - \frac{P_{RE}}{V_{ac}}) + I_L \sin \varphi_L \\ K (I_L \cos \varphi_L - \frac{P_{RE}}{V_{ac}}) \\ K_b (I_L \cos \varphi_L - \frac{P_{RE}}{V_{ac}}) \end{bmatrix} \quad (11)$$

where

$$\begin{bmatrix} K_a \\ K_b \end{bmatrix} = \begin{bmatrix} \tan(\frac{\pi}{6} - \varphi_a)(1 - K) \\ \tan(\frac{\pi}{6} + \varphi_b)K \end{bmatrix} \quad (12)$$

### 3 Analysis of Two Compensation Strategies for Co-phase Systems

#### 3.1 Full Compensation Strategy

In the literature, the full compensation strategy is widely applied in the co-phase system. According to [6], this is defined as such that both negative sequence current and reactive power injected to the three-phase power grid are all zeros. In this paper, in order to take into account of the effect of power factors to the power quality and the converter capacity, the definition of full compensation is slightly modified. Three-phase power factors are allowed to vary in the range according to the grid code while the negative sequence current is limited to zero. In this modified full compensation scheme, three-phase currents and voltages are still balanced, thus the phasor sum of  $\tilde{I}_a + \tilde{I}_b + \tilde{I}_c = 0$ , and  $I_a = I_b = I_c$ . However a certain amount of reactive power can be injected into the power grid. Accordingly, under the slightly modified full compensation strategy, the phase angles can be predefined as  $\varphi_a = \varphi_b = \varphi_c = \varphi$ , (9) can thus be revised as (13).

$$\tan \varphi = \frac{\sin \varphi}{\cos \varphi} = \frac{-I_a \sin(\frac{\pi}{3} - \varphi) + I_b \sin(\frac{\pi}{3} + \varphi)}{I_a \cos(\frac{\pi}{3} - \varphi) + I_b \cos(\frac{\pi}{3} + \varphi)} \quad (13)$$

With these pre-defined phase angles, the full power compensation factor  $K_{full}$  can be evaluated using (10). The balanced phasor diagram is shown in Fig. 2(c).

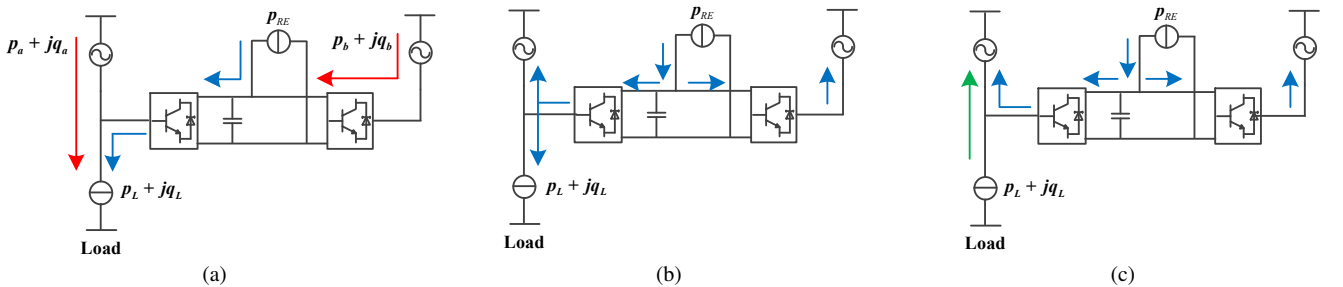


**Fig. 3:** Power flow diagrams. (a) Operation mode 1. (b) Operation mode 2. (c) Operation mode 3.

$$\begin{bmatrix} I_{ap} \\ I_{aq} \\ I_{cap} \\ I_{caq} \\ I_{cbp} \\ I_{cbq} \end{bmatrix} = \begin{bmatrix} I_L \cos \varphi_L - \frac{N_2}{N_1} I_{cbp} - \frac{P_{RE}}{V_{ac}} \\ \tan\left(\frac{\pi}{6} - \varphi_a\right) \left( I_L \cos \varphi_L - \frac{N_2}{N_1} I_{cbp} - \frac{P_{RE}}{V_{ac}} \right) \\ \frac{N_2}{N_1} I_{cbp} + \frac{P_{RE}}{V_{ac}} \\ I_L \sin \varphi_L + \tan\left(\frac{\pi}{6} - \varphi_a\right) \left( I_L \cos \varphi_L - \frac{N_2}{N_1} I_{cbp} - \frac{P_{RE}}{V_{ac}} \right) \\ I_{cbp} \\ \tan\left(\frac{\pi}{6} + \varphi_b\right) I_{cbp} \end{bmatrix} \quad (8)$$

$$\begin{aligned} I_{cbp} &= y(\varphi_a, \varphi_b, \varphi_c) \\ &= \frac{\cos\left(\frac{5\pi}{6} - \varphi_b\right) \left( \sin \varphi_c \sin\left(\frac{\pi}{6} + \varphi_a\right) + \cos \varphi_c \cos\left(\frac{\pi}{6} + \varphi_a\right) \right) \left( I_L \cos \varphi_L - \frac{P_{RE}}{V_{ac}} \right)}{\sin \varphi_c \left( \cos\left(\frac{\pi}{6} - \varphi_a\right) \cos\left(\frac{\pi}{3} + \varphi_b\right) + \sin\left(\frac{\pi}{6} + \varphi_a\right) \cos\left(\frac{5\pi}{6} - \varphi_b\right) \right) - \cos \varphi_c \left( \cos\left(\frac{\pi}{6} - \varphi_a\right) \sin\left(\frac{\pi}{3} + \varphi_b\right) - \cos\left(\frac{\pi}{6} + \varphi_a\right) \cos\left(\frac{5\pi}{6} - \varphi_b\right) \right)} \\ &= K(\varphi_a, \varphi_b, \varphi_c) \cdot \left( I_L \cos \varphi_L - \frac{P_{RE}}{V_{ac}} \right) \end{aligned} \quad (10)$$

### 3.2 Optimal Compensation Strategy Based on NSGA-II Algorithm

In this section, an optimal compensation strategy, instead of the full compensation strategy presented in the aforementioned subsection, is presented based on NSGA-II. The aim is to search for a set of phase angles  $\varphi_a, \varphi_b, \varphi_c$ , which can lead to reducing the operating capacity of HPQC while meeting the power quality requirements, rather than presetting these phase angles in the full compensation strategy. This is a multi-objective optimization problem, which can generally be formulated as follows:

$$\begin{aligned} \min \quad & F = \{f_1(x), \dots, f_m(x)\} \\ \text{s.t.} \quad & h_r(x) = 0 \quad r = 1, \dots, N_r \\ & g_s(x) \leq 0 \quad s = 1, \dots, N_s \\ & x^T = [x_1, \dots, x_I] \\ & x_{imin} \leq x_i \leq x_{imax} \quad i = 1, 2, \dots, I \end{aligned} \quad (14)$$

where  $F$  is the overall objective function,  $f_i (i = 1, \dots, m)$  are individual objective functions,  $h_r$  and  $g_s$  are equality and inequality constraints respectively,  $x_{imin}$  and  $x_{imax}$  are the lower and upper limits of decision variables  $x_i (i = 1, \dots, I)$ . In the three-phase power supply system, the voltage unbalance ratio  $\varepsilon_u$ , which is defined in (15), is used to evaluate the unbalance of the traction power system. Generally speaking, the voltage unbalance is not supposed to exceed 2% [26].

$$\varepsilon_u = \frac{\sqrt{3} |I^-| U_L}{S_c} \times 100\% \leq 2\% \quad (15)$$

where  $|I^-|$  is the negative sequence current of the three-phase power grid,  $S_c$  is the short-circuit capacity and  $U_L$  is the line-to-line voltage. From (15),  $|I^-|$  is deduced in (16).

$$|I^-| \leq \frac{2\% \cdot S_c}{\sqrt{3} U_L} \quad (16)$$

$|I^-|$  can be calculated by (17).

$$|I^-| = \left| \tilde{I}_a + \tilde{I}_b \cdot e^{j\frac{4\pi}{3}} + \tilde{I}_c \cdot e^{j\frac{2\pi}{3}} \right| \quad (17)$$

The HPQC includes the rectifier part and inverter part. Thus the operating capacity  $S$  of HPQC is defined as

$$S = U_{ac} I_{ca} + U_{bc} I_{cb} \quad (18)$$

Since the traction loads and renewable energy are predictable based on the existing information such as timetable and historic data, they can be taken as known a priori in the optimization. Thus from (2), (8) and (11), the negative sequence current and operating capacity can be expressed as the function of variables  $\varphi_a, \varphi_b$  and  $\varphi_c$ , i.e.  $|I^-| = f_1(\varphi_a, \varphi_b, \varphi_c)$  and  $S = f_2(\varphi_a, \varphi_b, \varphi_c)$ .

For the co-phase system, the operating capacity  $S$  and negative sequence current  $|I^-|$  are both expected to be minimized. By choosing suitable phase angles  $(\varphi_a, \varphi_b, \varphi_c)$  and controlling compensation currents, it is feasible to achieve optimal compensation control for given traction loads and renewable power injection. Further, the three-phase power factors are supposed to be within the range of 0.95 to 1 according to the grid code, i.e.  $-18.19^\circ \leq \varphi_a, \varphi_b, \varphi_c \leq 18.19^\circ$ . Taking this power factor range and (16) as the constraints, the co-phase system compensation design can be formulated as the following constrained multi-objective optimization problem:

$$\begin{aligned} \min \quad & \begin{cases} |I^-| = f_1(\varphi_a, \varphi_b, \varphi_c) \\ S = f_2(\varphi_a, \varphi_b, \varphi_c) \end{cases} \\ \text{s.t.} \quad & \begin{cases} |I^-| = f_1(\varphi_a, \varphi_b, \varphi_c) \leq \frac{2\% \cdot S}{\sqrt{3} U_L} \\ 0.95 \leq \arccos(\varphi_i) \leq 1 \quad (i = a, b, c) \end{cases} \end{aligned} \quad (19)$$

NSGA-II is an improved fast non-dominate sorting strategy based on the genetic algorithm. Compared to the original NSGA, NSGA-II has the following distinctive features [27]:

- In NSGA-II, a crowded comparison approach is used to replace the original sharing function approach in NSGA. Thus, NSGA-II does not require any user-defined parameter for maintaining diversity among population members.
- NSGA-II has a computational complexity of  $O(MN^2)$  (where  $M$  is the number of objectives and  $N$  is the population size). While the overall computational complexity of the original NSGA is  $O(MN^3)$ .
- The elitism strategy is adopted in NSGA-II, which can speed up convergence of the algorithm significantly and help preventing the loss of good solutions.

Extensive research has already demonstrated the outstanding performance and convergence speed of the NSGA-II in solving a broad range of multi-objective optimization problems. Fig. 4 shows the flowchart of the NSGA-II. The whole procedure of NSGA-II includes several steps: 1) Initialize parent population of size  $N$ ; 2) Produce offspring by genetic operations and merge parent population into a new population of size  $2N$ ; 3) Evaluate the fitness of individual solutions and select  $N$  better individuals as a new parent population; 4) Termination criterion judgment.

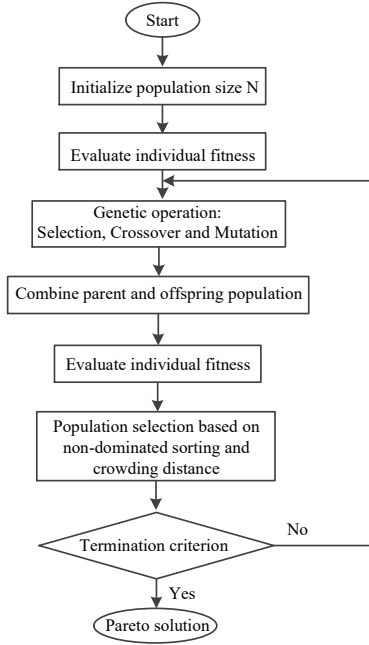


Fig. 4: Flowchart of NSGA-II algorithm

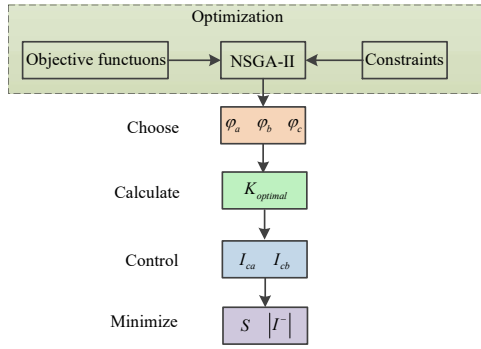


Fig. 5: Process of optimal control

The goal of the multi-objective optimization is to identify the Pareto front which is also called as Pareto optimal solutions. For the problem in (19), NSGA-II will produce the Pareto front from which a set of optimal phase angles ( $\varphi_a, \varphi_b, \varphi_c$ ) are selected. This optimal set of phase angles is then applied to (10), hence the optimal power compensation factor  $K_{optimal}$  is calculated. Subsequently the compensation currents  $I_{ca}$  and  $I_{cb}$  can be calculated based on (11) to achieve the optimal compensation. The whole process of the optimal compensation control is shown in Fig. 5.

## 4 A Hybrid Optimal Compensation Control

The previous section presents an optimal operation scheme for the co-phase system based on the assumptions that the traction load and the renewable generation are known a prior based on some prediction models. However, in reality, these prediction models may not be accurate enough. Therefore, to countermeasure the prediction errors in real time applications, this section proposes and presents a hybrid optimal control scheme based on NSGA-II, which combines both the proposed optimal compensation and full compensation. In the proposed hybrid optimal compensation control scheme, the full compensation scheme is used to eliminate the negative sequence current produced due to the prediction error, while the optimal compensation introduced in section 3 is deployed to achieve the operating capacity reduction.

### 4.1 Reference Current Calculation

In the hybrid optimal compensation control, a step is to calculate the reference current. This paper introduces an effective reference current calculation method based on the instantaneous power analysis approach introduced in [12]. Using this method, based on the required traction power, the real-time reference currents can be calculated for both the full compensation scheme (using full compensation factor  $K_{full}$ ) or optimal compensation scheme (using optimal compensation factor  $K_{optimal}$ ). The single-phase traction load instantaneous power is given by (20).

$$\begin{bmatrix} p \\ q \end{bmatrix} = \begin{bmatrix} V_{ac} & V_{ac}e^{-j\frac{\pi}{2}} \\ V_{ac}e^{-j\frac{\pi}{2}} & -V_{ac} \end{bmatrix} \begin{bmatrix} I_L \\ I_L e^{-j\frac{\pi}{2}} \end{bmatrix} \quad (20)$$

Based on (11), the real-time power of HPQC is expressed as (21).

$$\begin{bmatrix} p_{ca} \\ q_{ca} \\ p_{cb} \\ q_{cb} \end{bmatrix} = \begin{bmatrix} K(p - P_{RE}) + P_{RE} \\ K_a(p - P_{RE}) + q \\ K(p - P_{RE}) + p^* \\ K_b((p - P_{RE}) + p^*) \end{bmatrix} \quad (21)$$

where compensation factor  $K$  can either be  $K_{full}$ , hence implementing the full compensation. Or, if  $K$  is set to  $K_{optimal}$ , then the optimal compensation is implemented. The inverse transformation of (20) is used for reference current calculation, yielding (22).

$$\begin{cases} I_{ca}^* = \frac{V_{ac}p_{ca} + V_{ac}e^{-j\frac{\pi}{2}}q_{ca}}{V_{ac}^2 + (V_{ac}e^{-j\frac{\pi}{2}})^2} \\ I_{cb}^* = \frac{V_{bc}p_{cb} + V_{bc}e^{-j\frac{\pi}{2}}q_{cb}}{V_{bc}^2 + (V_{bc}e^{-j\frac{\pi}{2}})^2} \end{cases} \quad (22)$$

The control block is shown in Fig. 6. The PI controller is used to stabilize the DC-link voltage.

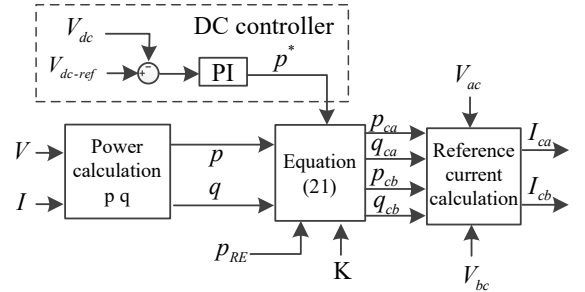
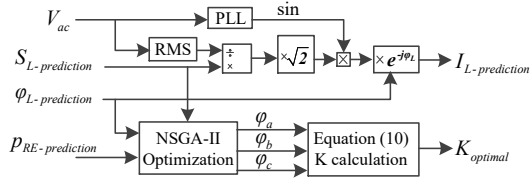


Fig. 6: Reference current calculation

### 4.2 Real-time Current Synchronization and Calculation of Optimal Compensation Factor K

As illustrated in section 3, the traction load  $S_L$  and its power factor angle  $\varphi_L$  can be predicted in advance. Then the real-time current  $I_L$  can be predicted using (23) and needs to be synchronized for instantaneous power calculation. A phase-locked loop (PLL) is employed to achieve the phase synchronization of voltage  $V_{ac}$ . Based on the predicted renewable  $P_{RE}$ , the optimal compensation factor  $K_{optimal}$  can be also obtained. The control diagram is shown in Fig. 7, where  $I_{L-prediction}$  stands for predicted load current,  $S_{L-prediction}$  for predicted traction load, and  $\varphi_{L-prediction}$  for predicted power factor angle.

$$I_{L-prediction} = \frac{\sqrt{2}S_{L-prediction}}{V_{ac}} \sin(\omega t - \frac{\pi}{6} - \varphi_L) \quad (23)$$



**Fig. 7:** Real-time current synchronization and  $K_{optimal}$  calculation

### 4.3 Hybrid Optimal Compensation Control

The NSGA-II based optimal compensation depends on the prediction accuracy of the traction loads and renewable energy. If the prediction error is not considered in the control design, it is highly likely that the negative sequence current will exceed the limit.

Fig. 8 illustrates the hybrid optimal compensation control scheme, which combines both the optimal compensation scheme and the full compensation branch. The latter is used to estimate and correct the errors in the converter reference currents which are initially determined using the optimal compensation scheme and based on the predicted traction and renewable powers. The whole procedure is summarized as follows: 1) Compare the real-time measured renewable power  $P_{RE}$  and traction current  $I_L$  and their corresponding predicted values, then calculate the current and power differences,  $\Delta I_L$  and  $\Delta P_{RE}$  respectively. 2) Based on  $\Delta I_L$  and measured voltage  $V_{ac}$ , calculate instantaneous error power  $\Delta p_L$  and  $\Delta q_L$  according to (20). 3) As stated in section 3.1, for the traditional full compensation scheme, the three phase angles are set as  $\varphi_a = \varphi_b = \varphi_c = 0^\circ$ . Hence based on (10), the full compensation factor  $K_{full}$  can be calculated as 0.5. 4) Substituting  $K_{full}$  and  $\Delta P_{RE}$  to (21), the required additional compensation powers for the HPQC,  $\Delta p_{ca}$ ,  $\Delta q_{ca}$  and  $\Delta p_{cb}$ ,  $\Delta q_{cb}$  can be calculated. 5) These quantities are substituted in (22) to calculate the additional current  $\Delta I_{ca}$  and  $\Delta I_{cb}$ . 6) Finally the reference compensation currents can be obtained as

$$\begin{bmatrix} I_{ca}^* \\ I_{cb}^* \end{bmatrix} = \begin{bmatrix} I_{ca-prediction} + \Delta I_{ca} \\ I_{cb-prediction} + \Delta I_{cb} \end{bmatrix} \quad (24)$$

Note both  $I_{ca-prediction}$  and  $I_{cb-prediction}$  are calculated from the optimal compensation control, described in section 3.2.  $K_{optimal}$  is the optimal power compensation factor, calculated from (10), using the optimal set of  $(\varphi_a, \varphi_b, \varphi_c)$  optimized by NSGA-II. With this hybrid compensation scheme, no extra negative sequence current will be produced and the power quality of the three-phase power grid can always meet the requirements in the presence of prediction errors of the traction load and renewable power.

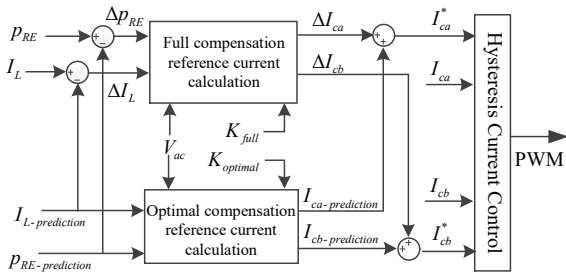


**Fig. 8:** Hybrid optimal compensation control

## 5 Simulation Studies

In order to verify the effectiveness of the proposed NSGA-II based optimal compensation and the control performance, a number of simulation experiments were conducted using Matlab/Simulink. The simulation schematic circuit is shown in Fig. 9. The traction loads and renewable energy are simulated as controllable current sources. The system parameters are listed in Table 1.

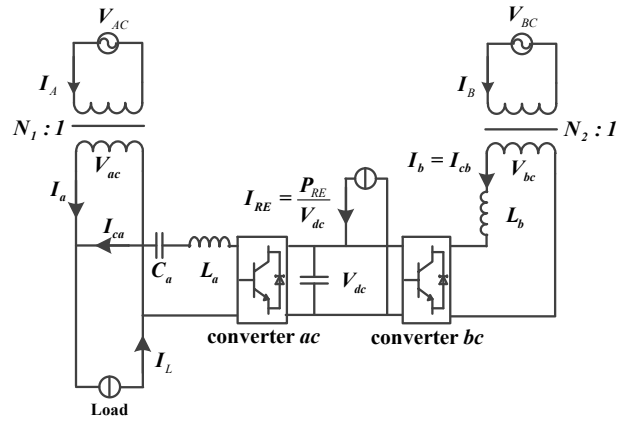


**Fig. 9:** Simulation schematic circuit

**Table 1** System simulation parameters

Items	Description
Three-phase line-to-line voltage $V_{AC}, V_{BC}$	190kV
Short circuit capacity $S_c$	500MVA
V/V transformer	60MVA 110kV/27.5kV
HPQC DC capacitor	10000 $\mu$ F
HPQC DC voltage	65kV
Phase ac coupling capacitance $C_a$	44.5 $\mu$ F
Phase ac coupling inductance $L_a$	50mH
Phase bc coupling inductance $L_b$	30mH

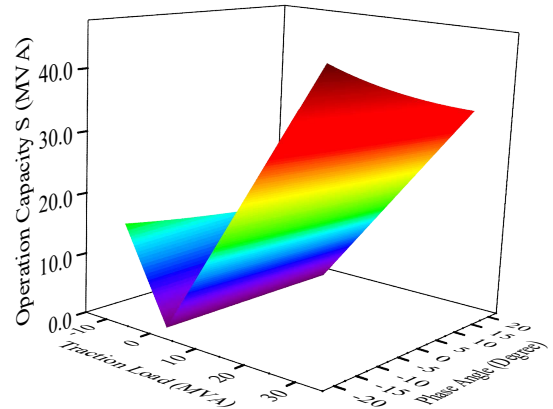


**Fig. 10:** Operating capacity comparison under full compensation with different phase angles

### 5.1 Comparison between Full Compensation and Optimal Compensation without Renewable Energy

In this section, the validity of NSGA-II based optimization is first verified without renewable energy. To emulate the characteristic of time-varying high-speed trains and different operation modes including traction and regeneration, the load power factor is set to 0.95. The traction loads are arranged as follows:

- 0~0.3s  $S_L = 0$
- 0.3s~0.55s  $S_L = 30$ MVA
- 0.55s~0.8s  $S_L = 15$ MVA
- 0.8s~1.05s  $S_L = 4$ MVA
- 1.05s~1.3s  $S_L = -10$ MVA
- 1.3s~1.4s  $S_L = 0$

For full compensation, as discussed in section 3.1,  $\varphi_a = \varphi_b = \varphi_c$  is required. The comparison of operating capacity with different phase angles is analyzed, as shown in Fig 10. It is evident that, compared to

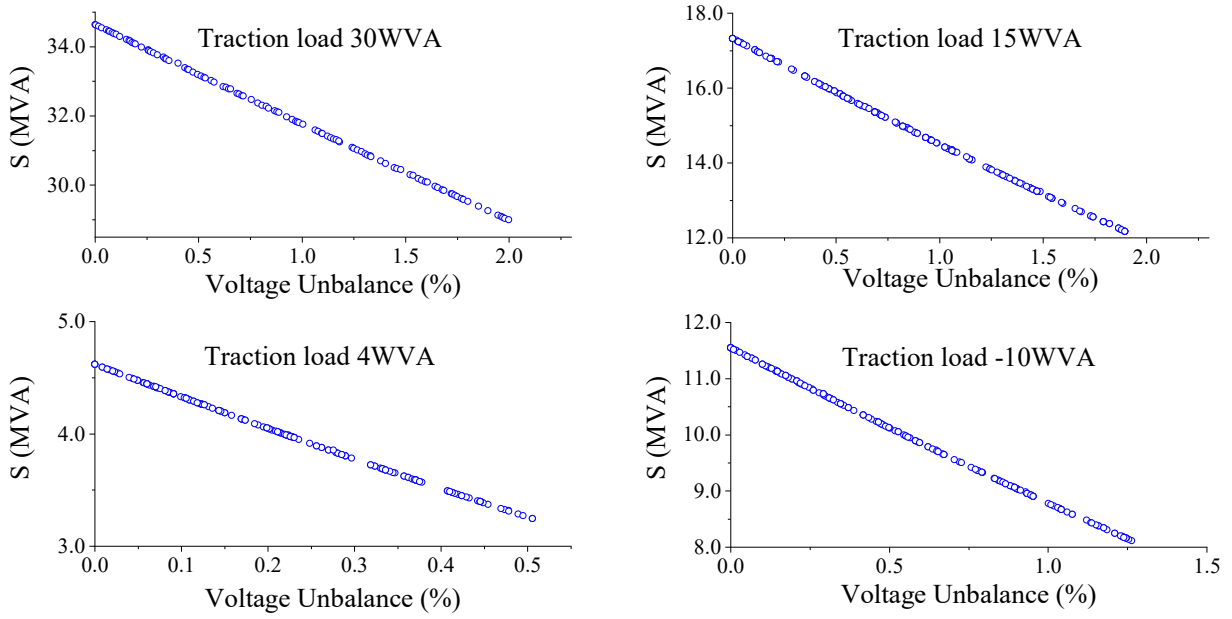


**Fig. 11:** Pareto optimal solutions for varying traction loads without renewable energy integration

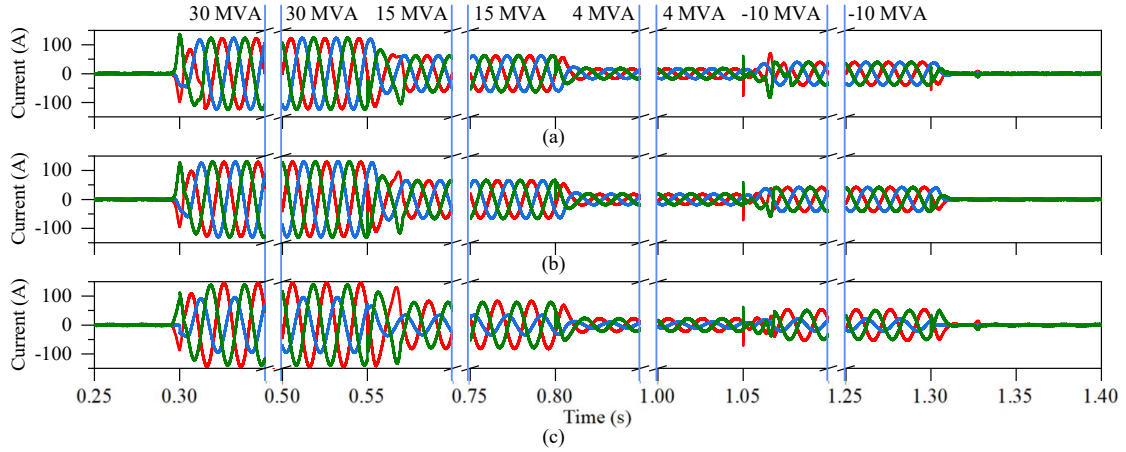


**Fig. 12:** Three-phase currents without renewable energy integration. (a) Full compensation  $\varphi = 0^\circ$ . (b) Full compensation  $\varphi = 18.19^\circ$ . (c) Optimal compensation.

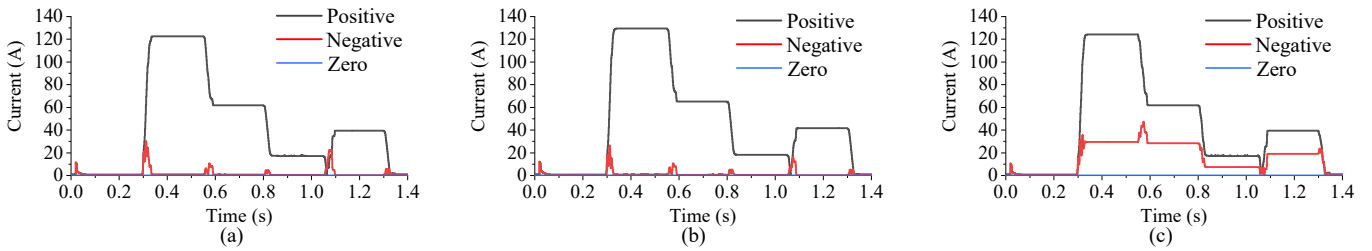


**Fig. 13:** Positive, negative and zero sequence currents without renewable integration (a) Full compensation  $\varphi = 0^\circ$ . (b) Full compensation  $\varphi = 18.19^\circ$ . (c) Optimal compensation.

the full compensation where  $\varphi_a = \varphi_b = \varphi_c = 0$ , the operating capacity is reduced for larger phase angles. That is due to the fact that the HPQC only provides part of the reactive power rather in full.

In the simulation, the total population of NSGA-II is set to 200 and iteration steps are 300. The crossover probability is 0.9 and the mutation probability is 0.2. By utilizing the NSGA-II algorithm for optimization, the Pareto optimal solutions are obtained as illustrated in Fig. 11. It is shown that the voltage unbalance of the power grid

is below the limit 2% for all traction loads. The solutions with the smallest operating capacity  $S$  are selected (see Table 2). In this way, the optimal operating capacity compensation is achieved.

The three-phase currents shown in Fig. 12(a)-(c) corresponding to the full and optimal compensation schemes are the grid side currents  $I_A$ ,  $I_B$  and  $I_C$  in Fig. 1. The stable-state currents are ignored here. For full compensation, two cases with  $\varphi = 0^\circ$  and  $\varphi = 18.19^\circ$  are adopted. In Fig. 13(a), (b) and (c), the black, red and blue lines

represent positive sequence, negative sequence and zero sequence currents respectively. According to (16) and the parameters listed in Table 1, the limit of negative sequence current is calculated to be 30.4A. Under full compensation, the negative sequence currents are almost zero and three-phase currents are balanced for all traction loads, which are illustrated in Fig. 12(a)-(b) and Fig. 13(a)-(b). Under optimal compensation, the three-phase currents in Fig. 12(c) are unbalanced but the negative sequence currents for all traction loads are below the limit except for the allowed transient overshoot (see Fig. 13(c)). The results meet the control expectation.

The operating capacity comparison of HPQC is shown in Fig. 14. The black line and red line correspond to the full compensation strategy with  $\varphi = 0^\circ$  and  $\varphi = 18.19^\circ$  respectively. Under full compensation, when  $\varphi = 0^\circ$ , the reactive power provided by the three-phase power grid is zero. However, choosing the phase angle  $\varphi = 18.19^\circ$  leads to the operating capacity reduction, which is consistent with previous results. The blue line represents the optimal operating capacity compensation. It can be seen, compared to full compensation with  $\varphi = 0^\circ$ , that the operating capacity of

HPQC is reduced for all traction loads after optimization. The operating capacity reduction ratio for varying traction loads is 25.8%, 35.9%, 35.8% and 38.0% respectively, with an average of 33.9%. The maximum capacity reduction reaches 10.1 MVA.

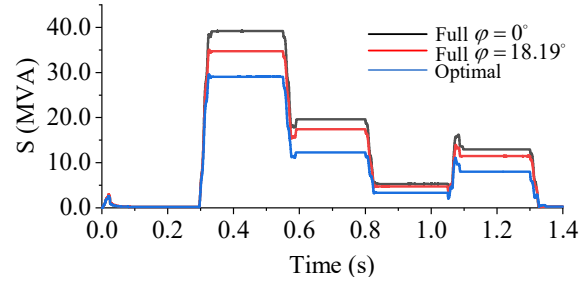


**Fig. 14:** Comparison of operating capacity without renewable energy integration

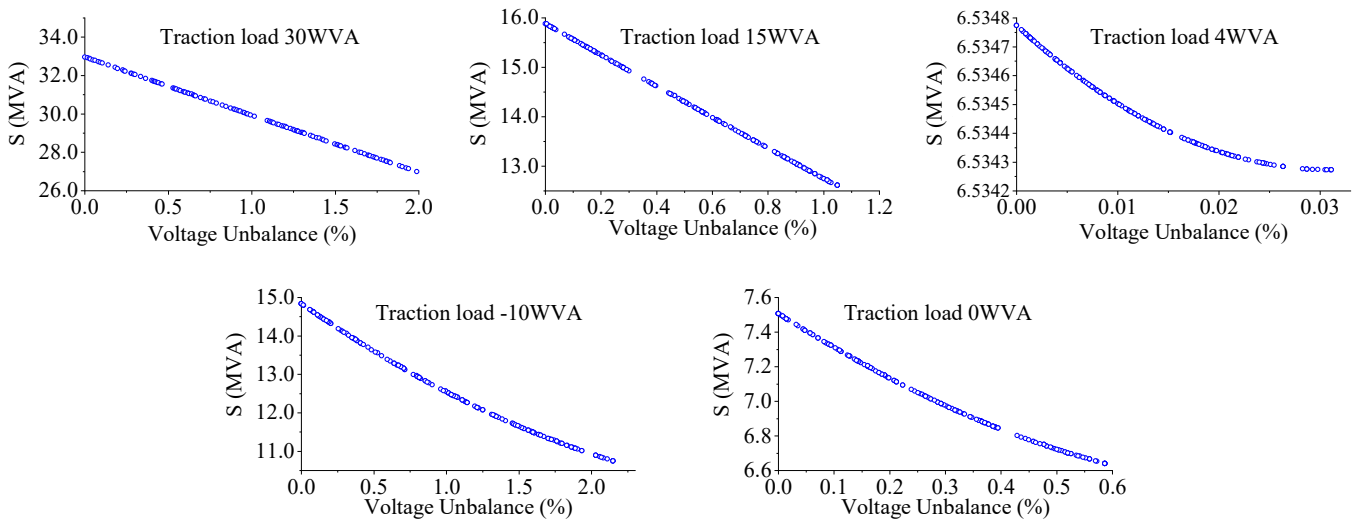


**Fig. 15:** Pareto optimal solutions for varying traction load with renewable 6.5MW

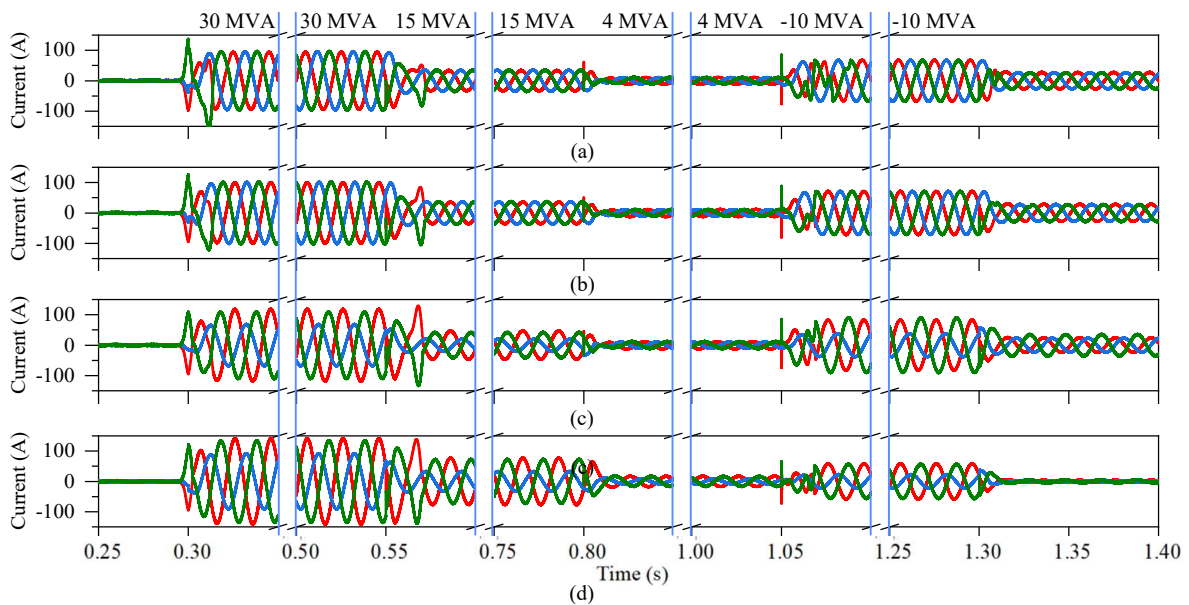


**Fig. 16:** Three-phase currents with renewable energy integration. (a) Full compensation  $\varphi = 0^\circ$  with renewable 6.5MW. (b) Full compensation  $\varphi = 18.19^\circ$  with renewable 6.5MW. (c) Optimal compensation with renewable 6.5MW. (d) Optimal compensation with renewable 1MW.

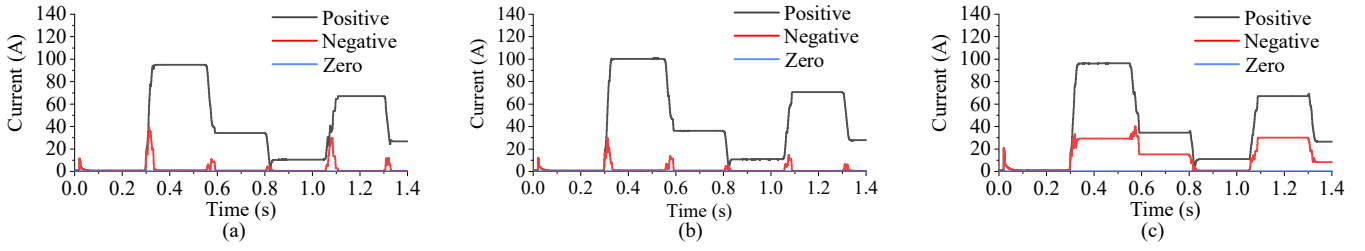


**Fig. 17:** Positive, negative and zero sequence currents (Renewable 6.5MW) (a) Full compensation  $\varphi = 0^\circ$ . (b) Full compensation  $\varphi = 18.19^\circ$ . (c) Optimal compensation.

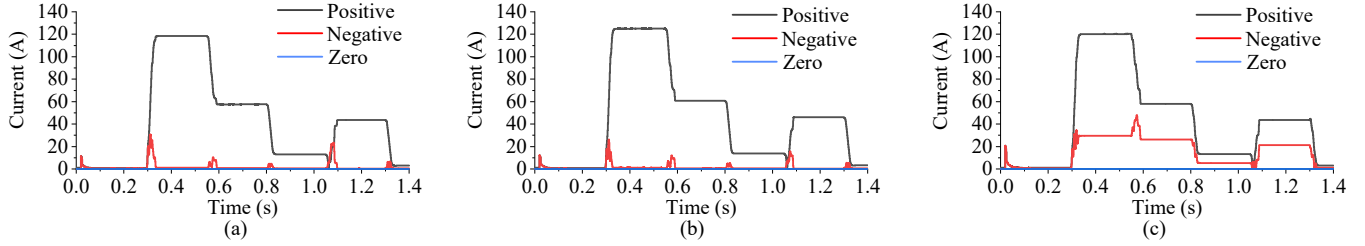


**Fig. 18:** Positive, negative and zero sequence currents (Renewable 1MW) (a) Full compensation  $\varphi = 0^\circ$ . (b) Full compensation  $\varphi = 18.19^\circ$ . (c) Optimal compensation.

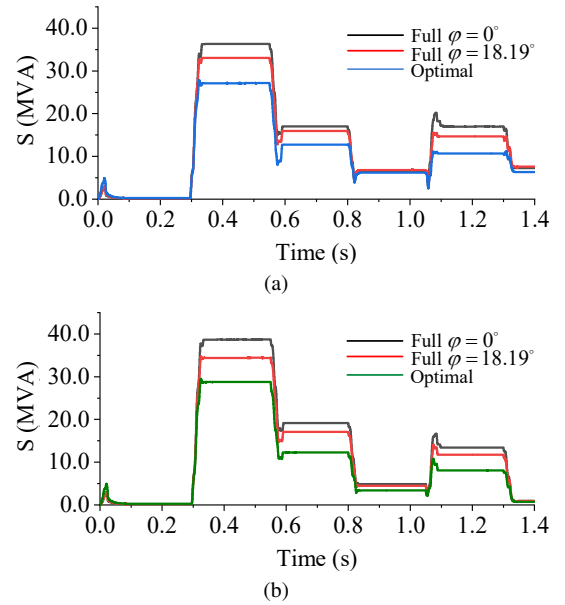
### 5.2 Comparison between Full Compensation and Optimal Compensation with Renewable Energy Integration

In the simulation, the renewable power of 6.5MW and 1MW are applied at 0.3s. Since renewable energy varies slowly compared to the traction loads in reality, the renewable energy is simulated as a constant current source which only provides active power. The traction loads are the same as section 5.1. After 1.3s, the traction load is zero and the renewable is fed to the power grid. The three operation modes discussed in section 2.2 are all included in simulation.

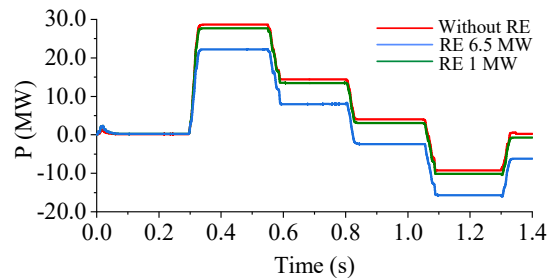
After optimization by NSGA-II, the Pareto solutions for renewable energy 6.5MW are acquired and shown in Fig. 15. The optimal phase angles are listed in Table 2. The three-phase grid side currents are shown in Fig. 16(a)-(d) including full and optimal compensation with renewable generations 6.5MW and 1MW. Note that the transient period shown in Fig. 12 and Fig. 16 is due to the sudden change of operation mode. The PI controller used for the DC-link voltage and current control, also with large filter inductors, slow the response speed. The negative sequence currents shown in Fig. 17 and Fig. 18 are below the limit under either full or optimal compensation.

For both cases with two renewable power 6.5MW and 1MW, the comparison results of both full compensation and optimal compensation are shown in Fig. 19(a) and (b). With renewable energy integration, the optimal compensation strategy based on NSGA-II still shows its effectiveness in operating capacity reduction. Compared to full compensation with  $\varphi = 0^\circ$ , when renewable energy is 6.5MW, the operating capacity reduction is 25.3%, 25.3%, 3.2%, 37.1% and 13.7%, with an average 20.9%. The maximum reduction in capacity is 9.2MVA. When renewable energy is 1MW, the capacity reduction are 25.6%, 35.9%, 20.4%, 39.6% and 22.2%. The average reduction ratio is 28.7% and the maximum reduction in capacity is 9.9MVA. According to Fig. 14 and Fig. 19, it is evident that when renewable energy is integrated, the operating capacity will not increase significantly and can even be reduced under the optimal compensation scheme. The difference only appears when the traction load is small or zero. In this scenario, almost all operating capacity of HPQC is used for feeding renewable power to the grid, rather than for traction load compensation.

Under the optimal compensation strategy, Fig. 20 illustrates the active power provided by the power grid at different cases. It is obvious that, when renewable energy is integrated, the reduced power from the power grid is approximately equal to the power from renewable energy, which shows the benefit of renewable energy integration for the traction power system. In the co-phase system, the power grid



**Fig. 19:** Comparison of operating capacity with renewable integration. (a) Renewable 6.5MW. (b) Renewable 1MW.

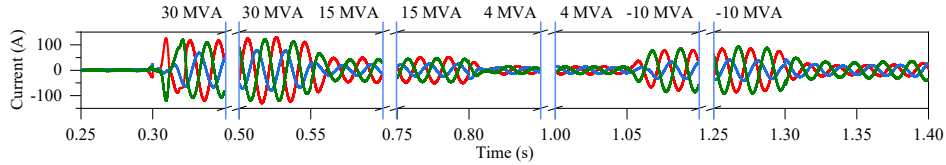


**Fig. 20:** Active power from three-phase power grid

and renewable energy are combined and work together for the traction loads. On the one hand, renewable energy integration makes the

**Table 2** Optimization results based on NSGA-II

Traction Load	30MVA	15MVA	4MVA	-10MVA	0MVA
Without renewable	$\varphi_a = 18.190^\circ$ $\varphi_b = 11.565^\circ$ $\varphi_c = -2.953^\circ$ $K = 0.3322$	$\varphi_a = 18.190^\circ$ $\varphi_b = 7.579^\circ$ $\varphi_c = -18.190^\circ$ $K = 0.2454$	$\varphi_a = 18.190^\circ$ $\varphi_b = 7.579^\circ$ $\varphi_c = -18.190^\circ$ $K = 0.2454$	$\varphi_a = 18.190^\circ$ $\varphi_b = 7.579^\circ$ $\varphi_c = -18.190^\circ$ $K = 0.2454$	
Renewable 6.5MW	$\varphi_a = 18.190^\circ$ $\varphi_b = 13.295^\circ$ $\varphi_c = -8.006^\circ$ $K = 0.2950$	$\varphi_a = 18.190^\circ$ $\varphi_b = 18.190^\circ$ $\varphi_c = -18.190^\circ$ $K = 0.2153$	$\varphi_a = -14.851^\circ$ $\varphi_b = -18.190^\circ$ $\varphi_c = -18.190^\circ$ $K = 0.5712$	$\varphi_a = 18.190^\circ$ $\varphi_b = -14.092^\circ$ $\varphi_c = -18.190^\circ$ $K = 0.3043$	$\varphi_a = 18.190^\circ$ $\varphi_b = -18.190^\circ$ $\varphi_c = -0.001^\circ$ $K = 0.5000$
Renewable 1MW	$\varphi_a = 18.190^\circ$ $\varphi_b = 12.003^\circ$ $\varphi_c = -3.698^\circ$ $K = 0.3294$	$\varphi_a = 18.190^\circ$ $\varphi_b = 9.925^\circ$ $\varphi_c = -18.190^\circ$ $K = 0.2389$	$\varphi_a = 18.190^\circ$ $\varphi_b = 15.625^\circ$ $\varphi_c = -18.190^\circ$ $K = 0.2229$	$\varphi_a = 18.190^\circ$ $\varphi_b = 3.902^\circ$ $\varphi_c = -18.190^\circ$ $K = 0.2553$	$\varphi_a = 18.190^\circ$ $\varphi_b = -18.190^\circ$ $\varphi_c = -0.024$ $K = 0.4998$

**Fig. 21:** Three-phase currents in the presence of prediction error (Renewable 6.5MW).

traction power supply system less dependent on the power grid, even it can become profitable by feeding excessive power to the grid. On the other hand, HPQC can not only be used for traction load compensation but also for the power grid connection of renewable energy, which saves additional converter construction costs.

### 5.3 Validation of Hybrid Optimal Control In the Presence of Prediction Error

In this part, the performance of hybrid optimal control in the presence of prediction error is tested. The real-time error is introduced into the predictions of the traction loads and renewable energy (6.5MW). The three-phase currents with prediction error are shown in Fig. 21. The maximum error of traction loads and renewable energy is 5MVA and 1MW respectively, which is shown in Fig. 22(a) and (b). The black and red lines represent the prediction power, and the actual power which includes prediction error.

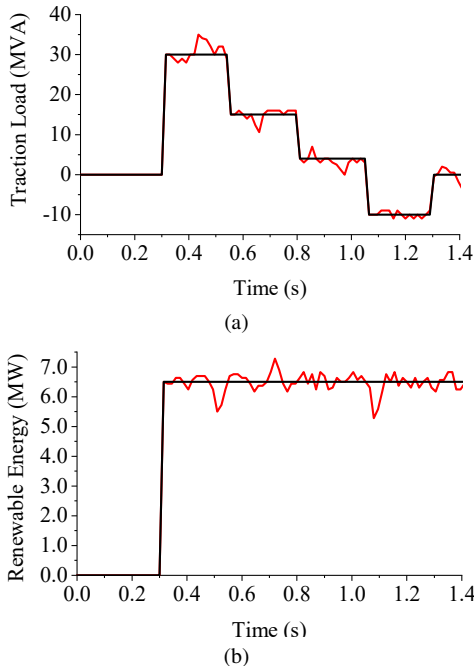
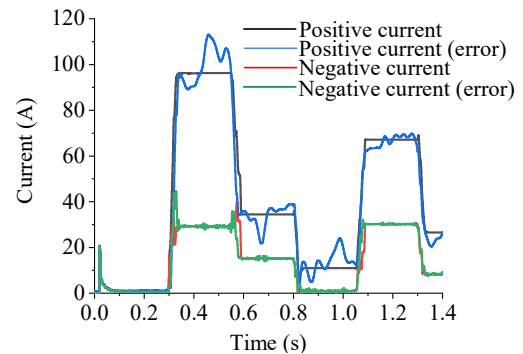
**Fig. 22:** Prediction errors. (a) Load error. (b) Renewable error.

Fig. 23 shows the comparison of the positive and negative sequence currents. It is noted that the positive sequence current with prediction error is unstable but the negative sequence current is almost the same as the current in which no prediction error exists. This implies that no extra negative sequence current is produced and injected into the three-phase power grid with the hybrid optimal control. The results verify that even in the presence of prediction errors, the voltage unbalance is still  $< 2\%$ .

## 6 Conclusion

In this paper, an optimization strategy based on NSGA-II algorithm has been proposed for the co-phase system with renewable energy integration. A hybrid optimal compensation control has been developed to eliminate the negative sequence current caused by real-time prediction error. Extensive simulation experiments have been conducted to verify the effectiveness of the proposed NSGA-II based optimal compensation strategy. It has revealed that, compared with the full compensation strategy, the optimal compensation achieves better performance than traditional full compensation scheme regardless the renewable is integrated or not. The operating capacity of HPQC is reduced and the power quality requirements are met. The simulation experiments show that the proposed method can achieve an average operating capacity reduction of more than 20%. Further, renewable energy integration decreases the power demand from the power grid. When the prediction error is considered, the traction power system unbalance will not become worse under the hybrid optimal compensation control.

**Fig. 23:** Comparison of positive and negative sequence currents

## 7 References

- 1 Ronanki, D., Singh, S.A., Williamson, S.S.: 'Comprehensive topological overview of rolling stock architectures and recent trends in electric railway traction systems', *IEEE Transactions on Transportation Electrification*, 2017, **3**, (3), pp. 724–738
- 2 Mousavi Gazafzudi, S.M., Tabakhpour Langerudy, A., Fuchs, E.F., Al-Haddad, K.: 'Power quality issues in railway electrification: A comprehensive perspective', *IEEE Transactions on Industrial Electronics*, 2015, **62**, (5), pp. 3081–3090
- 3 Hu, H., Shao, Y., Tang, L., Ma, J., He, Z., Gao, S.: 'Overview of harmonic and resonance in railway electrification systems', *IEEE Transactions on Industry Applications*, 2018, **54**, (5), pp. 5227–5245
- 4 Tao, H., Hu, H., Zhu, X., Zhou, Y., He, Z.: 'Harmonic instability analysis and suppression method based on  $\alpha\beta$  frame impedance for trains and network interaction system', *IEEE Transactions on Energy Conversion*, 2019, **34**, (2), pp. 1124–1134
- 5 Gotham, D.J., Heydt, G.T.: 'Power flow control and power flow studies for systems with facts devices', *IEEE Transactions on Power Systems*, 1998, **13**, (1), pp. 60–65
- 6 Shu, Z., Xie, S., Li, Q.: 'Single-phase back-to-back converter for active power balancing, reactive power compensation, and harmonic filtering in traction power system', *IEEE Transactions on Power Electronics*, 2011, **26**, (2), pp. 334–343
- 7 Xie, B., Li, Y., Zhang, Z., Hu, S., Zhang, Z., Luo, L., et al.: 'A compensation system for cophase high-speed electric railways by reactive power generation of shc sac', *IEEE Transactions on Industrial Electronics*, 2018, **65**, (4), pp. 2956–2966
- 8 Shu, Z., Xie, S., Lu, K., Zhao, Y., Nan, X., Qiu, D., et al.: 'Digital detection, control, and distribution system for co-phase traction power supply application', *IEEE Transactions on Industrial Electronics*, 2013, **60**, (5), pp. 1831–1839
- 9 Shirahama, H., Muto, T.: 'A novel power loss calculation method for power converters by transforming switching-loss into impulse-waveforms'. In: 2018 21st International Conference on Electrical Machines and Systems (ICEMS). (, 2018. pp. 2226–2229
- 10 Sadigh, A.K., Dargahi, V., Corzine, K.A.: 'Analytical determination of conduction and switching power losses in flying-capacitor-based active neutral-point-clamped multilevel converter', *IEEE Transactions on Power Electronics*, 2016, **31**, (8), pp. 5473–5494
- 11 Gbadega, P.A., Saha, A.K.: 'Loss assessment of mmc-based vsc-hvdc converters using iec 62751-1-2 std. and component datasheet parameters'. In: 2018 IEEE PES/IAS PowerAfrica. (, 2018. pp. 1–9
- 12 Dai, N., Wong, M., Lao, K., Wong, C.: 'Modelling and control of a railway power conditioner in co-phase traction power system under partial compensation', *IET Power Electronics*, 2014, **7**, (5), pp. 1044–1054
- 13 Chen, M., Li, Q., Roberts, C., Hillmansen, S., Tricoli, P., Zhao, N., et al.: 'Modelling and performance analysis of advanced combined co-phase traction power supply system in electrified railway', *IET Generation, Transmission Distribution*, 2016, **10**, (4), pp. 906–916
- 14 Lao, K., Dai, N., Liu, W., Wong, M.: 'Hybrid power quality compensator with minimum dc operation voltage design for high-speed traction power systems', *IEEE Transactions on Power Electronics*, 2013, **28**, (4), pp. 2024–2036
- 15 Dai, N.Y., Lao, K., Lam, C.: 'Hybrid railway power conditioner with partial compensation for converter rating reduction', *IEEE Transactions on Industry Applications*, 2015, **51**, (5), pp. 4130–4138
- 16 Lao, K., Wong, M., Dai, N., Lam, C., Wang, L., Wong, C.: 'Analysis of the effects of operation voltage range in flexible dc control on railway hpqc compensation capability in high-speed co-phase railway power', *IEEE Transactions on Power Electronics*, 2018, **33**, (2), pp. 1760–1774
- 17 Xiao, W., El Moursi, M.S., Khan, O., Infield, D.: 'Review of grid-tied converter topologies used in photovoltaic systems', *IET Renewable Power Generation*, 2016, **10**, (10), pp. 1543–1551
- 18 D'Arco, S., Piegari, L., Tricoli, P.: 'Comparative analysis of topologies to integrate photovoltaic sources in the feeder stations of ac railways', *IEEE Transactions on Transportation Electrification*, 2018, **4**, (4), pp. 951–960
- 19 Wu, M., Wang, W., Deng, W., Chen, H., Dai, C., Chen, W.: 'Back-to-back pv generation system for electrified railway and its control strategy'. In: 2017 IEEE Transportation Electrification Conference and Expo, Asia-Pacific (ITEC Asia-Pacific). (, 2017. pp. 1–6
- 20 Rageh, M., Ndtoungou, A., Hamadi, A., Al-Haddad, K.: 'Railway traction supply with pv integration for power quality issues'. In: IECON 2018 - 44th Annual Conference of the IEEE Industrial Electronics Society. (, 2018. pp. 1436–1441
- 21 Zhu, X., Hu, H., Tao, H., He, Z.: 'Stability analysis of pv plant-tied mvdc railway electrification system', *IEEE Transactions on Transportation Electrification*, 2019, **5**, (1), pp. 311–323
- 22 Aguado, J.A., Sánchez Racero, A.J., de la Torre, S.: 'Optimal operation of electric railways with renewable energy and electric storage systems', *IEEE Transactions on Smart Grid*, 2018, **9**, (2), pp. 993–1001
- 23 Pereira, L.A., Haffner, S., Nicol, G., Dias, T.F.: 'Multiobjective optimization of five-phase induction machines based on nsga-ii', *IEEE Transactions on Industrial Electronics*, 2017, **64**, (12), pp. 9844–9853
- 24 Li, X., Dong, H., Li, H., Li, M., Sun, Z.: 'Optimization control of front-end speed regulation (fesr) wind turbine based on improved nsga-ii', *IEEE Access*, 2019, **7**, pp. 45583–45593
- 25 Li, Y., Lu, X., Kar, N.C.: 'Rule-based control strategy with novel parameters optimization using nsga-ii for power-split phev operation cost minimization', *IEEE Transactions on Vehicular Technology*, 2014, **63**, (7), pp. 3051–3061
- 26 IEEE: 'IEEE recommended practice and requirements for harmonic control in electric power systems', *IEEE Std 519-2014 (Revision of IEEE Std 519-1992)*, 2014, pp. 1–29
- 27 Deb, K., Pratap, A., Agarwal, S., Meyarivan, T.: 'A fast and elitist multiobjective genetic algorithm: Nsga-ii', *IEEE Transactions on Evolutionary Computation*, 2002, **6**, (2), pp. 182–197